The Astrophysical Journal, 835:200 (9pp), 2017 February 1 doi:10.3847/1538-4357/835/2/200

Characterization of the Wolf 1061 Planetary System

Stephen R. Kane[1], Kaspar von Braun[2], Gregory W. Henry[3], Miranda A. Waters[1], Tabetha S. Boyajian[4], and Andrew W. Mann[5]
[1] Department of Physics & Astronomy, San Francisco State University, 1600 Holloway Avenue, San Francisco, CA 94132, USA; skane@sfsu.edu
[2] Lowell Observatory, 1400 West Mars Hill Road, Flagstaff, AZ 86001, USA
[3] Center of Excellence in Information Systems, Tennessee State University, 3500 John A. Merritt Blvd., Box 9501, Nashville, TN 37209, USA
[4] Department of Physics & Astronomy, Louisiana State University, Baton Rouge, LA 70803, USA
[5] Department of Astronomy, University of Texas at Austin, Austin, TX 78712, USA
Received 2016 November 27; revised 2016 December 22; accepted 2016 December 22; published 2017 January 31

Abstract

A critical component of exoplanetary studies is an exhaustive characterization of the host star, from which the planetary properties are frequently derived. Of particular value are the radius, temperature, and luminosity, which are key stellar parameters for studies of transit and habitability science. Here we present the results of new observations of Wolf 1061, known to host three super-Earths. Our observations from the Center for High Angular Resolution Astronomy interferometric array provide a direct stellar radius measurement of $0.3207 \pm 0.0088\ R_{\odot}$, from which we calculate the effective temperature and luminosity using spectral energy distribution models. We obtained 7 yr of precise, automated photometry that reveals the correct stellar rotation period of 89.3 ± 1.8 days, finds no evidence of photometric transits, and confirms that the radial velocity signals are not due to stellar activity. Finally, our stellar properties are used to calculate the extent of the Habitable Zone (HZ) for the Wolf 1061 system, for which the optimistic boundaries are 0.09–0.23 au. Our simulations of the planetary orbital dynamics show that the eccentricity of the HZ planet oscillates to values as high as ∼0.15 as it exchanges angular momentum with the other planets in the system.

Key words: astrobiology – planetary systems – stars: individual (Wolf 1061) – techniques: radial velocities

1. Introduction

It is frequently stated that we understand exoplanets only as well as we understand the host star. Such a statement is particularly true for low-mass dwarf stars, whose atmospheres often diverge from blackbody models. There has been a concerted effort in recent years to obtain observational constraints on the stellar models for low-mass stars (Boyajian et al. 2012; Mann et al. 2015), especially for those monitored by the *Kepler* mission (Muirhead et al. 2012, 2014; Huber et al. 2014; Gaidos et al. 2016). A further challenge includes the confusion that can be caused by the stellar rotation period of low-mass stars since that can often coincide with the range of orbital periods of planets that may exist in the Habitable Zone (HZ) of those stars (Newton et al. 2016b; Vanderburg et al. 2016). Even so, there have been several successful detections of terrestrial planets in or near the HZ of low-mass stars, such as Kepler-186 f (Quintana et al. 2014), K2-3 d (Crossfield et al. 2015), and the recently discovered Proxima Centauri b (Anglada-Escudé et al. 2016).

The low-mass M-dwarf star Wolf 1061 (also designated as GJ 628) is one of our closest neighbors, located approximately 4.3 pc away (van Leeuwen 2007). The star was recently discovered to host three planets that lie within the super-Earth mass regime, one of which may be located within the HZ of the system (Wright et al. 2016). The orbits of the planets were significantly updated by Astudillo-Defru et al. (2016a) using additional data from the High Accuracy Radial velocity Planet Searcher (HARPS) spectrograph. The orbital solutions largely agree with respect to the inner two planets, but the Astudillo-Defru et al. (2016a) solution finds an orbital period of the outer planet that is a factor of ∼3 larger than that found by Wright et al. (2016). Both of the solutions do agree that planet c is near or in the HZ of the host star, the location of which is highly dependent on the star parameters of luminosity and effective temperature. Both solutions also predict reasonably high transit probabilities and depths such that follow-up photometry during calculated transit windows is encouraged.

This paper presents a characterization of the Wolf 1061 host star and the associated planets with new data and numerical simulations. In Section 2, the fundamental stellar parameters of the host star are updated through interferometry data that provide measurements of the stellar radius, effective temperature, and luminosity. Section 3 presents 7 yr of precise, automated photometry that reveals the correct stellar rotation period, supports the existence of the three purported planets, and finds no evidence for planetary transits. The revised stellar parameters are utilized in Section 4 with a calculation of the system HZ and a dynamical simulation that shows variation of eccentricities for the planetary orbits. We provide a concluding discussion of the results in Section 5.

2. Fundamental Stellar Parameters

Wolf 1061 has been an object of interest for quite some time, primarily because of its high proper motion of 1191.5 ± 0.9 mas yr^{-1} (Davison et al. 2015) and its membership in the solar neighborhood. Despite its relatively close position to our star, the stellar properties of Wolf 1061 have remained uncertain, largely due to the fact that it is a very dim M3V late-type dwarf. Prior to our investigation, the values of Wolf 1061's temperature, luminosity, flux, and radius have varied in the literature. Previous estimates for the red dwarf's temperature have been reported as being as low as 2877 K (Léger et al. 2015) to as high as 3400 K (Avenhaus et al. 2012), with a variety of values reported between these two extremes (Jenkins et al. 2009; Bailey et al. 2012; Önehag et al. 2012; Rojas-Ayala et al. 2012; Cantrell et al. 2013; Neves et al. 2014; Lindgren et al. 2016; Wright et al. 2016). Less extreme are the variations in radius, from 0.30 $R_{\odot}$ (Newton et al. 2016b) to

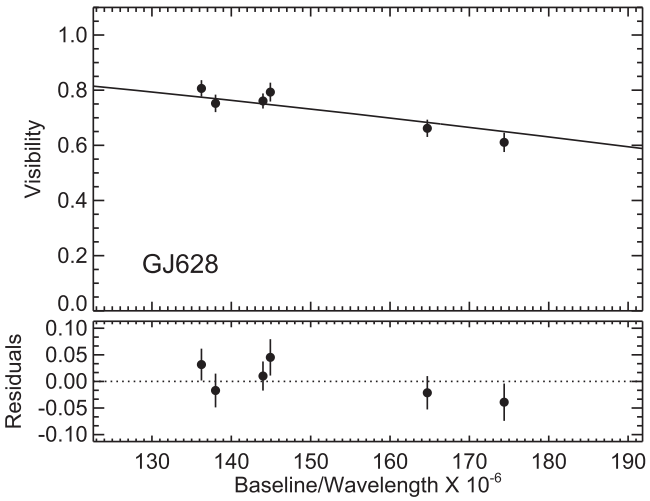

Figure 1. Calibrated visibility observations along with the limb-darkened angular diameter fit for Wolf 1061 (GJ 628) (top panel) and the fractional residuals around the fit (bottom panel). For more details, see Section 2.1.

Table 1
Stellar Parameters

Parameter	Value
V	10.07
B–V	1.57
Distance (pc)	4.29 ± 0.03
$F_{\rm BOL}$ (erg cm^{-2} s^{-1})	(1.920 ± 0.043) × 10^{-8}
$T_{\rm eff}$ (K)	3305 ± 46
$R_\star$ ($R_\odot$)	0.3207 ± 0.0088
$L_\star$ ($L_\odot$)	0.01102 ± 0.00027
$P_{\rm rot}$ (days)	89.3 ± 1.8

0.325 ± 0.012 $R_\odot$ (Mann et al. 2015), and in luminosity, which was previously reported to be 0.007870 $L_\odot$ (Wright et al. 2016). Precise determination of these essential characteristics has taken on new importance in light of the early 2016 discovery that Wolf 1061 is host to three exoplanets (Astudillo-Defru et al. 2016a; Wright et al. 2016).

2.1. Stellar Radius

Wolf 1061 was observed on 2016 June 30 and August 3–4, using the Georgia State University Center for High Angular Resolution Astronomy (CHARA) interferometric array (ten Brummelaar et al. 2005). Observations were conducted in H band with the CHARA Classic beam combiner (Sturmann et al. 2003; ten Brummelaar et al. 2005) in single-baseline mode. To remove the influence of atmospheric and instrumental systematics, our interferometric observations consist of bracketed sequences of object and calibrator stars. Calibrators were chosen using the ASPRO tool[6] to be near-point-like sources of similar brightness to Wolf 1061, located at small angular distances from it, and observed directly before and after the target: HD 143459, HD 146254, HD 149013, and HD 153229. This procedure follows our requirements that we use at least two calibrators, two baselines, and data obtained during at least two nights (e.g., von Braun et al. 2014; Boyajian et al. 2015, and references therein).

[6] http://www.jmmc.fr/aspro

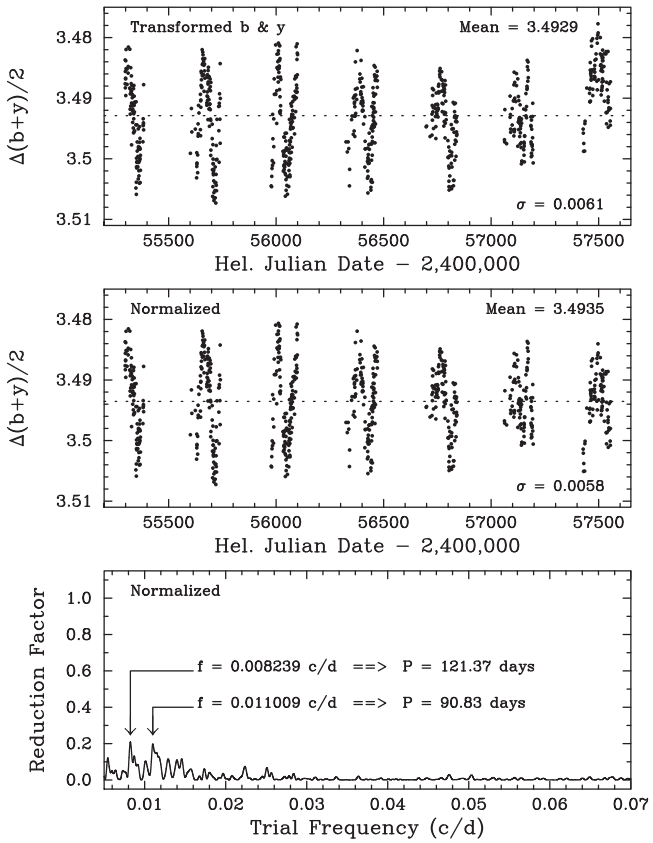

Figure 2. Top: 7 yr of photometric observations of Wolf 1061, comprising 756 nightly measurements, acquired with the T11 0.8 m APT at Fairborn Observatory. Slow rotational modulation of dark spots on the star's surface, as well as year-to-year evolution of the spot distribution, accounts for the brightness variability. The dotted line marks the mean brightness. Middle: the 756 observations are normalized so that all seasonal means are equal to the first, marked by the dotted line. Bottom: frequency spectrum of the complete normalized data set revealing low-amplitude variability at 121 or 91 days.

The uniform-disk and limb-darkened angular diameters ($\theta_{\rm UD}$ and $\theta_{\rm LD}$, respectively) are calculated by fitting the calibrated visibility measurements (Figure 1) to the respective functions for each relation. These functions may be described as nth-order Bessel functions of the angular diameter of the star, the projected distance between the two telescopes, and the wavelength of observation (Hanbury Brown et al. 1974).

We use the linear limb-darkening coefficient $\mu_H = 0.376$ from the PHOENIX models in Claret & Bloemen (2011) for stellar $T_{\rm eff} = 3000$ K and $\log g = 4.5$ to convert from $\theta_{\rm UD}$ to $\theta_{\rm LD}$. The uncertainties in the adopted limb-darkening coefficient amount to 0.2% when modifying the adopted gravity by 0.5 dex or the adopted $T_{\rm eff}$ by 200 K, well within the errors of our diameter estimate.

Our interferometric measurements produce the following values for Wolf 1061: $\theta_{\rm UD} = 0.674 \pm 0.018$ mas and $\theta_{\rm LD} = 0.695 \pm 0.018$ mas. Combined with the trigonometric parallax measurement of 232.98 ± 1.60 mas from van Leeuwen (2007), we obtain a stellar radius for Wolf 1061 of 0.3207 ± 0.0088 $R_\odot$, which is practically identical to the one estimated in Mann et al. (2015) of 0.325 ± 0.012 $R_\odot$.

2.2. Stellar Effective Temperature and Luminosity

To calculate Wolf 1061's effective temperature and luminosity, we perform a spectral energy distribution

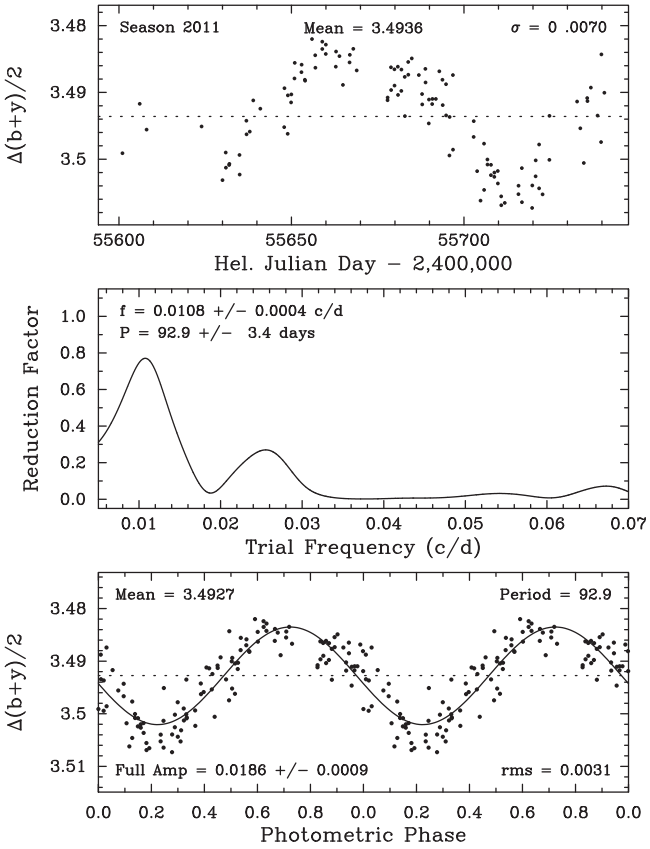

Figure 3. Top: JD plot of the 2011 observing season of Wolf 1061. Middle: frequency spectrum of the 2011 data giving a photometric period of 92.9 ± 3.4 days. Bottom: the 2011 data phased to the best period of 92.9 days and showing a peak-to-peak amplitude of 0.019 mag.

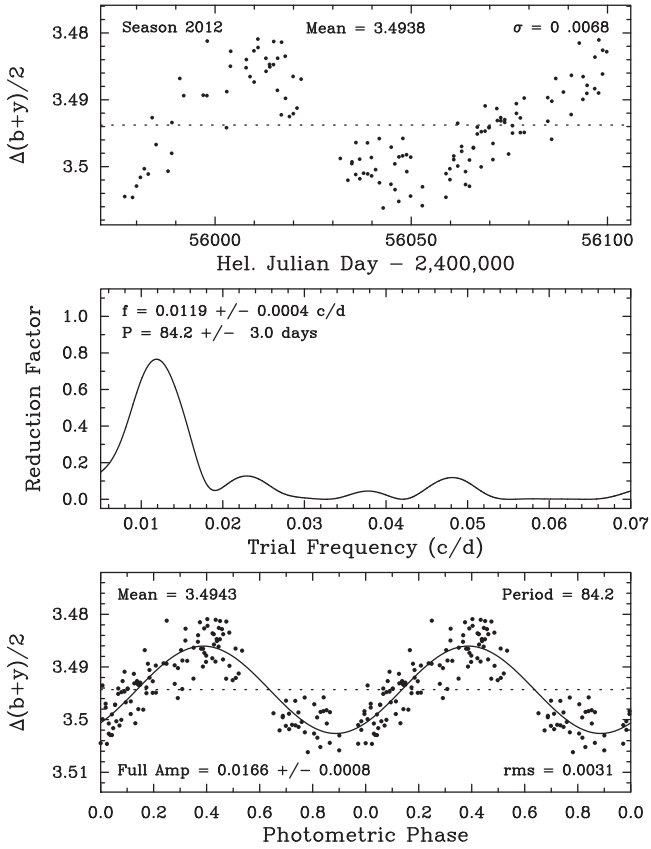

Figure 4. Same as Figure 3, except for the 2012 observing season, giving a period of 84.2 ± 3.0 days and a peak-to-peak amplitude of 0.017 mag.

(SED) fit based on spectrophotometry data obtained as part of the survey described in Mann et al. (2015); see in particular their Section 3. These spectrophotometry data have no color terms and only require a zero-point offset. We use literature photometry from Johnson & Harris (1954), Niconov et al. (1957), Johnson (1965), Corben et al. (1972), Veeder (1974), Mould & Hyland (1976), Cousins (1980a, 1980b), Reid (1982), Weis (1984), Mermilliod (1986), Weis (1986, 1987), Beichman et al. (1988), Laing (1989), Bessel (1990), Weis (1996), Koen et al. (2002), Cutri et al. (2003), Gautier et al. (2007), Kilkenny et al. (2007), Koen et al. (2010), Henden et al. (2012), Turnbull (2015), and Wright et al. (2016) to scale the spectrophotometry data and obtain the bolometric flux by simply integrating over wavelength. Interstellar reddening is set to zero in the fit, due to the close proximity of Wolf 1061. In the calculation of the bolometric flux, we use the modified filter profiles for the literature photometry from Mann & von Braun (2015) and use the 2% error correction described by Bohlin et al. (2014) to obtain realistic error estimates in $F_{\rm BOL}$. We calculate the following for Wolf 1061: $F_{\rm BOL} = (1.920 \pm 0.043) \times 10^{-8}$ erg cm^{-2} s^{-1}, $L = 0.01102 \pm 0.00027\ L_{\odot}$, and $T_{\rm eff} = 3305 \pm 46$ K. These values are consistent at $\lesssim 1\sigma$ with the ones in Table 5 of Mann et al. (2015) that use interferometric data for calibration of their semiempirical methods. Our stellar parameters for Wolf 1061, including the rotation period described in Section 3.1, are summarized in Table 1.

3. Photometric Observations

We have observed Wolf 1061 during its past seven observing seasons with the Tennessee State University (TSU) T11 0.80 m automatic photoelectric telescope (APT) at Fairborn Observatory in Arizona. Between 2010 April and 2016 June, the APT acquired 756 brightness measurements of Wolf 1061 on 464 different nights. Like other TSU APTs, T11 is equipped with a two-channel precision photometer designed and built by Louis Boyd at Fairborn. The photometer uses a dichroic filter and two EMI:9124QB bi-alkali photomultiplier tubes to separate and simultaneously measure the Strömgren b and y photometric passbands. Wolf 1061, designated here as the program star (P, $V = 10.10$, $B - V = 1.60$, M3.5V), was observed differentially with respect to three constant comparison stars HD 150177 (C1, $V = 6.33$, $B - V = 0.49$, F3V), HD 147753 (C2, $V = 7.58$, $B - V = 0.55$, F2V), and HD 148968 (C3, $V = 6.98$, $B - V = 0.14$, A0V). All differential magnitudes were corrected for extinction and transformed to the Strömgren photometric system. We computed final differential magnitudes of Wolf 1061 against the mean brightness of all three comparison stars as $P - (C1 + C2 + C3)/3_{by}$, where the subscript by indicates that we combined the Strömgren b and y observations into a single $(b + y)/2$ passband. The precision of a single observation from the T11 APT is typically 0.0015–0.0020 mag, determined by intercomparison of the comparison stars. Further details of our automatic telescopes, precision photometers, and observing and data reduction procedures can be found in Henry (1999) and Eaton et al. (2003) and references therein. Note that the T11 APT is essentially identical to the T8 APT described in Henry (1999).

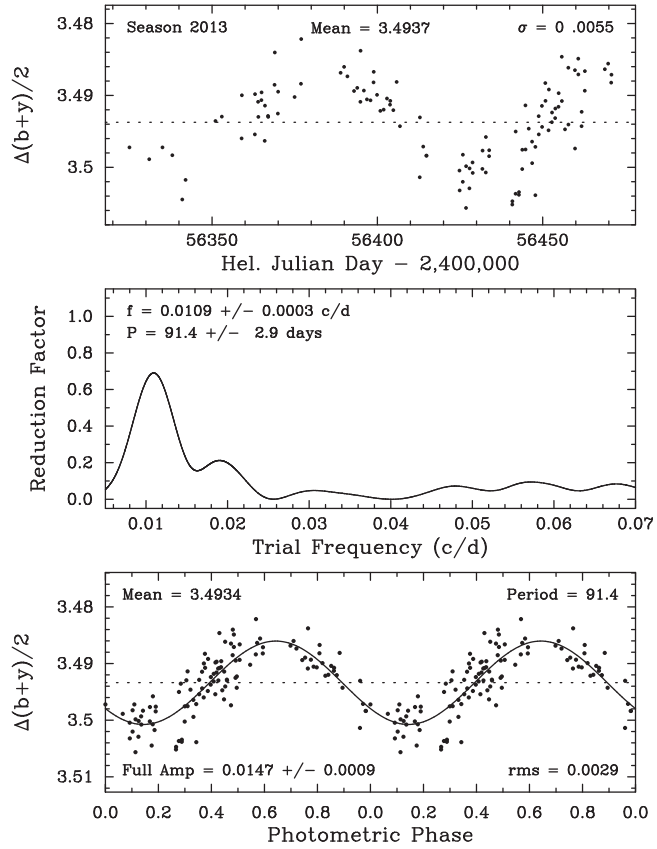

Figure 5. Same as Figure 3, except for the 2013 observing season, giving a best period of 91.4 ± 2.9 days and a peak-to-peak amplitude of 0.015 mag.

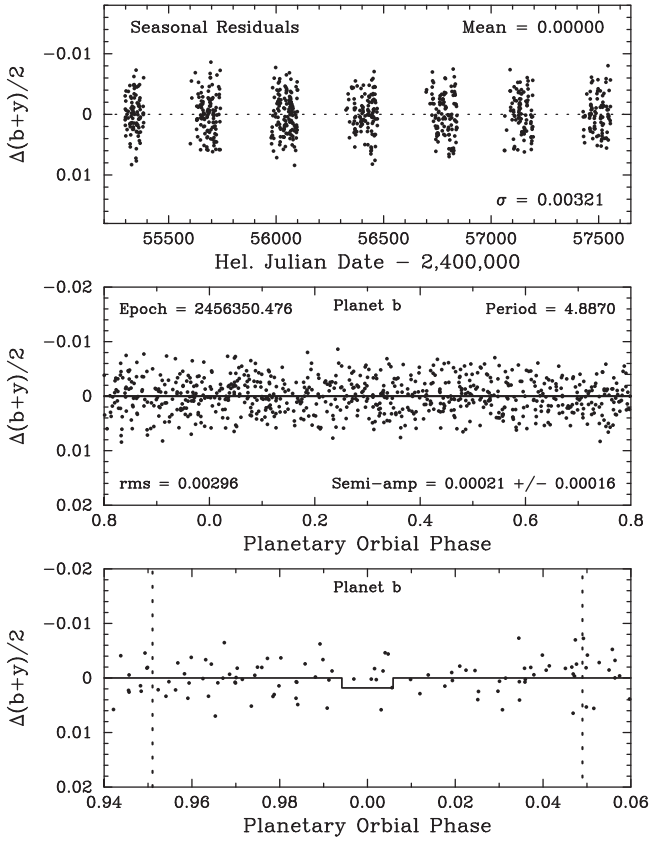

Figure 6. Top: residuals from the individual sine fits to the seven observing seasons of Wolf 1061 summarized in Table 2, plotted against Julian Date. Middle: residuals from the top panel phased with the 4.8870-day orbital period of planet b and time of conjunction derived from the radial velocities. A least-squares sine fit on the radial velocity period gives a semi-amplitude of just 0.00021 ± 0.00016 mag, establishing to high precision the lack of stellar activity on the radial velocity period and thus confirming the presence of stellar reflex motion caused by an orbiting planet. Bottom: close-up of the observations near the time of planetary conjunction at phase 0.0. The solid line shows a model transit computed from the parameters of planet b. The vertical lines mark the uncertainty in the predicted transit window. Our current photometric observations provide no evidence for transits.

3.1. Stellar Rotation Period

The final $P - (C1 + C2 + C3)/3_{by}$ differential magnitudes are plotted in the top panel of Figure 2 and show Wolf 1061 to be varying over a range of ∼0.02 mag with a timescale of ∼100 days. To remove the effects of the small year-to-year variations in mean brightness, we normalized the data shown in the middle panel of Figure 2 by adjusting the seven seasons so that each has the same mean as the first. A frequency spectrum of the normalized data is shown in the bottom panel. Weak periodicity is found around 91 and 121 days, both with amplitudes of a few millimagnitudes. The low amplitudes are due not only to the intrinsically low amplitude of Wolf 1061's photometric variability but also to year-to-year changes in the amplitude, shape, mean magnitude, and phase of minimum of the light curve. The 91- and 121-day periods are yearly aliases of each other caused by the large seasonal gaps in our light curve. We take the variability in Wolf 1061 to arise from the rotational modulation of a slowly evolving spot distribution on the photosphere of the star.

To determine the correct rotation period, we attempted a periodogram analysis of the seven individual observing seasons. Only the 2011, 2012, and 2013 observing seasons cover the light curve sufficiently well to give reliable results. Frequency spectra for these three observing seasons are shown in Figures 3–5. The complete results of our seasonal photometric analysis of Wolf 1061 are given in Table 2. Rotation periods and amplitudes that are poorly constrained are given in parentheses. The weighted mean of the 2011, 2012, and 2013 photometric periods is 89.3 ± 1.8 days. We identify this period as the true stellar rotation period and the 121-day period from Figure 2 as its yearly alias. This is consistent with the 93-day rotation period determined for Wolf 1061 by Astudillo-Defru et al. (2016b) from analyses of the Ca II H & K emission lines. Using the kinematic work of Newton et al. (2016a) for nearby M dwarfs, the rotation period suggests an age for Wolf 1061 of >5 Gyr.

However, as seen above in Figure 2, the rotational modulation of the light curve is not strictly sinusoidal over the 7 yr span of our observations. Therefore, stellar activity on the surface of Wolf 1061 might still be responsible for radial velocity variability, as has been demonstrated in other moderately active stars (see, e.g., Queloz et al. 2001; Paulson et al. 2004; Boisse et al. 2012).

3.2. Ruling Out Planetary Transits

We remove most of the photometric variability in Wolf 1061 by taking the residuals from the yearly sine fits specified in Table 2. These are plotted in the top panel of Figure 6. The standard deviation of the residuals from the mean (marked by the dotted line) is 0.0032 mag, roughly half the variability of the original light curve in the top panel of Figure 2. Periodogram analysis of the full set of residuals finds no significant periodicity.

Table 2
Summary of Photometric Observations for Wolf 1061

Observing Season (1)	N_{obs} (2)	Julian Date Range (HJD –2,400,000) (3)	Sigma (mag) (4)	P_{rot} (days) (5)	Full Amplitude (mag) (6)	$\langle P - (C1 + C2 + C3)/3_{by} \rangle$ (mag) (7)
2010	92	55297–55383	0.0061	(103.9)	(0.015)	3.4935 ± 0.0006
2011	117	55601–55740	0.0070	92.9 ± 3.4	0.0186 ± 0.0009	3.4936 ± 0.0006
2012	136	55976–56099	0.0068	84.2 ± 3.0	0.0166 ± 0.0008	3.4938 ± 0.0006
2013	115	56325–56470	0.0055	91.4 ± 2.9	0.0147 ± 0.0009	3.4937 ± 0.0005
2014	111	56698–56840	0.0050	(108.3)	(0.011)	3.4937 ± 0.0005
2015	93	57062–57195	0.0042	(58.7)	(0.008)	3.4936 ± 0.0004
2016	92	57428–57554	0.0045	(199.2)	(0.015)	3.4872 ± 0.0005

Note. Periods and amplitudes in parentheses are poorly determined.

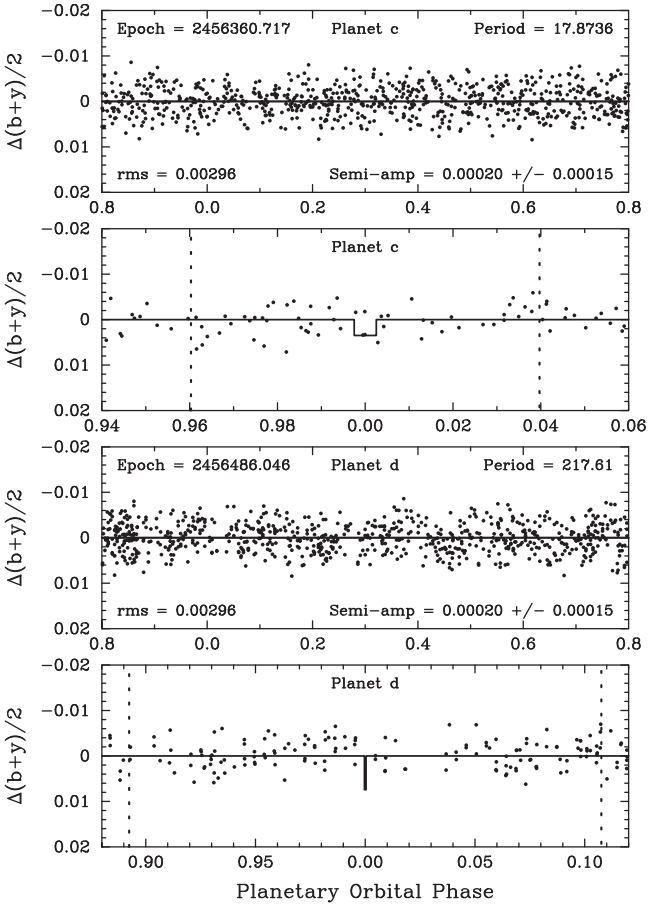

Figure 7. Same as Figure 6, but for Wolf 1061 c and d.

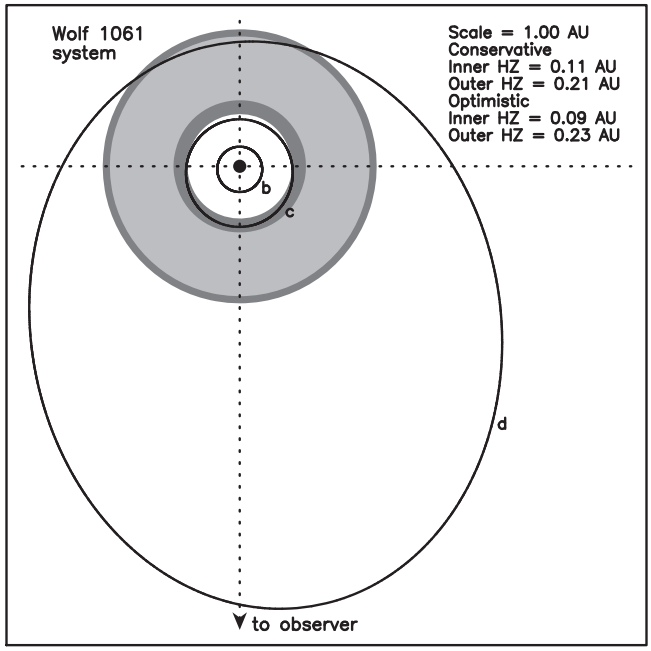

Figure 8. Top-down view of the Wolf 1061 system showing the orbits of the planets overlaid on the HZ. The extent of the HZ was calculated using the stellar parameters from Section 2.2. The physical scale depicted is 1.0 au on a side. The conservative HZ is shown as light gray, and the optimistic extension to the HZ is shown as dark gray.

The middle panel of Figure 6 shows the seasonal residuals phased with the 4.8870-day orbital period of Wolf 1061 b and the epoch of mid-transit from Table 4 of Astudillo-Defru et al. (2016a). A least-squares sinusoidal fit to the phased data gives a formal semi-amplitude of just 0.00021 ± 0.00016 mag, which limits any periodic brightness variability on the orbital period to a very small fraction of 1 mmag. This rules out the possibility that the 4.8870-day radial velocity variations are due to stellar activity. Instead, the lack of photometric variability confirms that the 4.8870-day radial velocity variations result from true planetary reflex motion.

The photometric observations within ±0.06 orbital phase of mid-transit are plotted with an expanded scale in the bottom panel of Figure 6. The solid curve shows the predicted transit phase (0.0), depth (0.00183 mag), and duration (0.057 days) of a central transit, computed from the stellar and planetary radii and the orbital elements of Wolf 1061 b. The vertical dotted lines give the $\pm 1\sigma$ uncertainty in the timing of the transit window, based on the uncertainties in the stellar radius provided in Section 2.1 and the improved orbital elements from Astudillo-Defru et al. (2016a). We find no evidence in our data for transits of planet b.

Results of similar analyses for planets c and d are shown in Figure 7. The low photometric amplitude of 0.00020 ± 0.00015 mag in the top panel confirms Wolf 1061 c as a planet since it shows that the radial velocity variations are not due to stellar activity. In the second panel, we find no evidence of photometric transits of planet c. The low amplitude of 0.00020 ± 0.00015 mag in the third panel confirms Wolf 1061 d as a planet. The bottom panel shows that we have insufficient data to rule out transits of planet d.

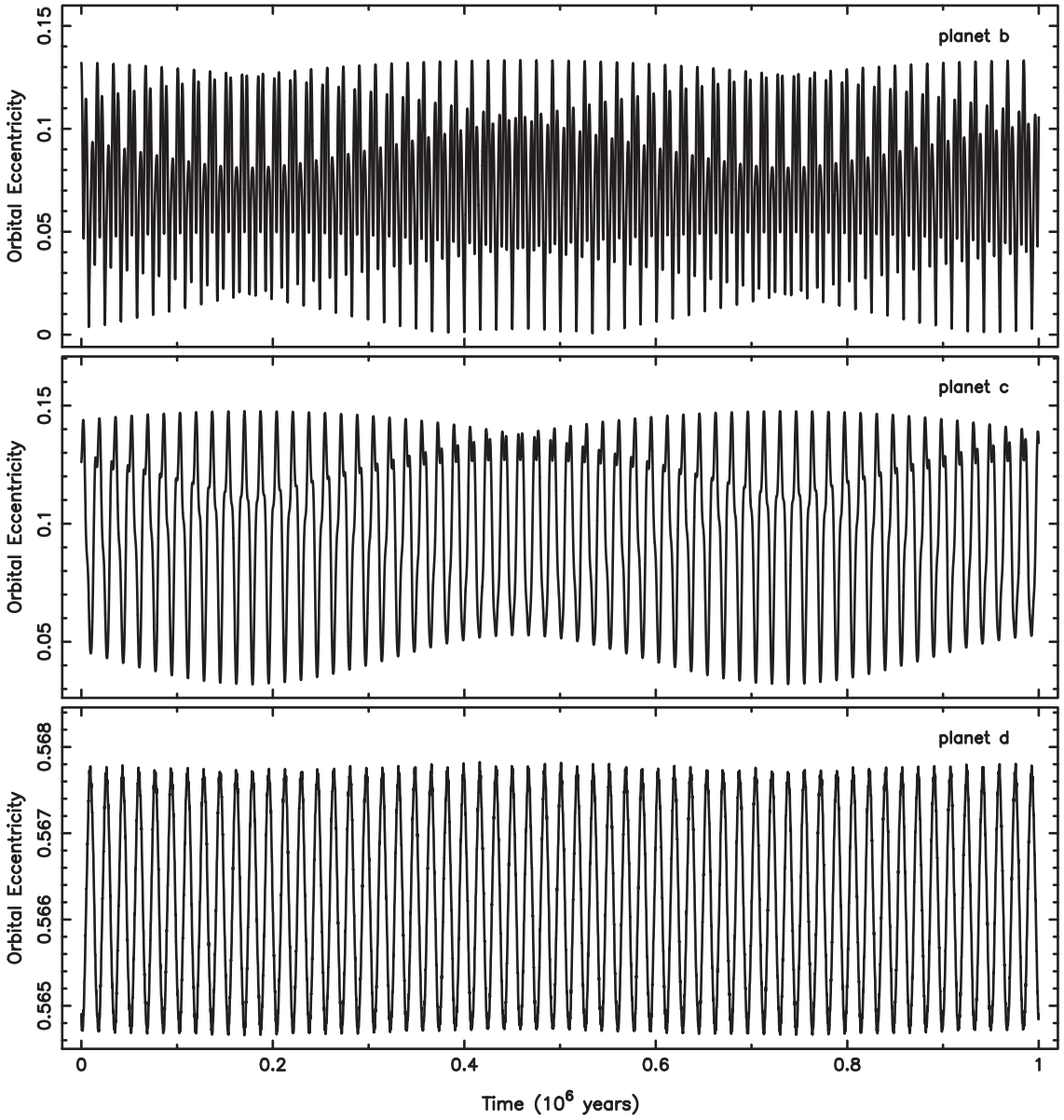

Figure 9. Eccentricity component of the orbital dynamics within the Wolf 1061 system, shown for planets b, c, and d (top, middle, and bottom panels, respectively).

4. Habitability of the System

Using the stellar parameters described above, we calculate the boundaries of the HZ and the long-term stability of the planets with respect to the HZ.

4.1. The HZ

The concept of the HZ as a target selection tool has been developed based on Earth climate models for several decades (Kasting et al. 1993, 2014). Specifically, the HZ defines the locations around a host star where the climate of an Earth analog will remain cool enough to avoid a runaway greenhouse effect and warm enough to prevent a runaway snowball effect. These calculations account for water absorption in the planetary atmosphere and stellar properties such as luminosity and effective temperature. To calculate the extent of the HZ, we use the methodology of Kopparapu et al. (2013, 2014). The "conservative" and "optimistic" HZ boundaries are calculated based on assumption regarding the time span over which the atmospheric evolutionary history of Venus and Mars allowed liquid water to remain on the surface. The catalog of confirmed planets and planetary candidates detected by the *Kepler* mission (Kane et al. 2016) describes the conservative and optimistic HZ boundaries in more detail.

Using the updated stellar parameters from this work (see Section 2.2), we estimate the inner and outer boundaries of the conservative HZ to be 0.11 and 0.21 au, respectively. Allowing for the optimistic conditions for surface liquid water, the inner and outer HZ boundaries are 0.09 and 0.23 au, respectively. Shown in Figure 8 is a top-down view of the planetary orbits in the Wolf 1061 system, using the orbital solution of Astudillo-Defru et al. (2016a). The conservative HZ is shown as light gray, and the optimistic extension to the HZ is shown as dark gray. The scale of the figure is 1.0 au on a side. The orbital eccentricities of the planets are 0.13, 0.13, and 0.57 for the b, c, and d planets, respectively. The outer planet passes briefly through the HZ during its periastron passage, spending 6% of the orbital period within the HZ. Planet c spends 61% of its

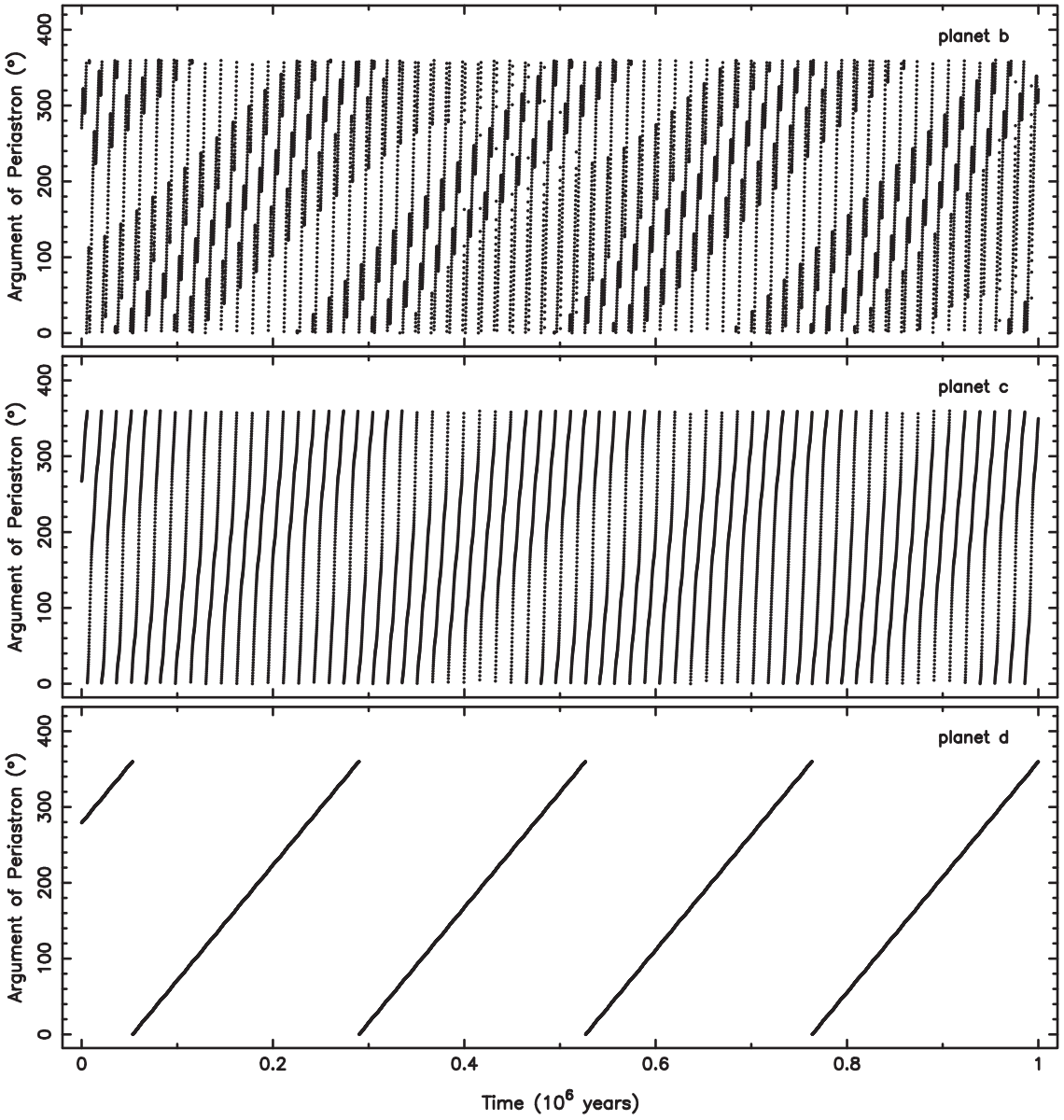

Figure 10. Argument-of-periastron component of the orbital dynamics within the Wolf 1061 system, shown for planets b, c, and d (top, middle, and bottom panels, respectively).

orbit duration within the HZ, but that time remains constrained to the optimistic HZ. In that respect, planet c is quite similar to the case of Kepler-69 c, which was proposed to be a strong super-Venus candidate by Kane et al. (2013). Indeed, both of the inner two planets, terrestrial in nature according to the results of both Wright et al. (2016) and Astudillo-Defru et al. (2016a), lie within the Venus Zone of the host star (Kane et al. 2014) and are thus possible runaway greenhouse candidates.

4.2. Orbital Stability and Dynamics

Another factor that plays a role in the habitability of the system is the orbital dynamics between the planets as a function of time. To investigate orbital stability and dynamics, we utilized the Mercury Integrator Package (Chambers 1999), with the hybrid symplectic/Bulirsch–Stoer integrator and a Jacobi coordinate system. The initial conditions were set using the orbital solution of Astudillo-Defru et al. (2016a) and the integration executed for a simulated duration of 10^7 yr. The time resolution was set to 0.1 days in order to adequately meet the recommended minimum time step criterion of 1/20 of the shortest system orbital period (Duncan et al. 1998). The orbital architecture of the system was output in 100 yr intervals.

For the coplanar scenario where the system is viewed approximately edge-on (inclination of $i = 90°$, and the true planetary masses are equivalent to the minimum masses), the system was found to be stable over the full 10^7 yr simulation duration. Although stable, the compact nature of the system, combined with the relatively large orbital eccentricities, results in an active dynamical evolution of key Keplerian orbital parameters. In particular, evidence of the angular momentum exchange between the planets can be observed in the oscillations of the eccentricity and argument of periastron. These evolutions of eccentricity and argument of periastron are shown for a simulation duration of 10^6 yr in Figures 9 and 10, respectively.

The bottom panel of Figure 9 shows that the amplitude of the eccentricity variations for the outer planet is largely insensitive to the presence of the inner planets and remains close to the initial value of $e_d = 0.565$. The interaction between the inner two planets is more pronounced, with mean eccentricities substantially below the initial values of $e_b = 0.132$ and $e_c = 0.126$. Similarly, the precession of the periastron arguments evolves on a rapid timescale for the inner two planets compared with the outer planet (see Figure 10). The eccentricity of the inner planet reduces to the circular case at regular intervals, whereas the eccentricity of planet c drops as low as ~0.03. The eccentricity of a planet within the HZ does not necessarily exclude the presence of liquid water on the surface, as the required conditions also depend on such factors as atmospheric composition, scale height, and response to variations in incident flux (Williams & Pollard 2002; Kane & Gelino 2012). However, it is worth noting that a zero eccentricity for planet c results in the orbit being entirely interior to the optimistic HZ. It is thus possible that planet c is more amenable to habitable conditions when near to peak eccentricity, since the planet moves slowly through the apastron passage in the HZ.

5. Conclusions

The assessment of host star properties is a critical component of exoplanetary studies, at least for the realm of indirect detections through which exoplanet discoveries thus far have predominantly occurred. This situation will remain true for the coming years, during which the transit method will primarily be used from space missions such as the *Transiting Exoplanet Survey Satellite*, the *CHaracterising ExOPlanet Satellite* (*CHEOPS*), and the *PLAnetary Transits and Oscillations of stars* (*PLATO*) mission. Of particular interest are the radius and effective temperature of the stars since the radius impacts the interpretation of observed transit events and the combination of radius and temperature is used to calculate the extent of the HZ.

Here we have presented the results from direct measurements of stellar properties for one of the closest known exoplanet host stars, Wolf 1061. Our direct measurement of the stellar radius from interferometric observations gives $0.3207 \pm 0.0088\ R_\odot$, which is remarkably close to the value previous calculated by Mann et al. (2015), which can be considered a significant triumph for the empirical calibrations used in that work. Our SED fit resulted in determining a luminosity of $L = 0.01102 \pm 0.00027\ L_\odot$ for Wolf 1061 and, after combination with the measured angular diameter, an effective temperature of $T_{\rm eff} = 3305 \pm 46$ K.

We further provide 7 yr of Wolf 1061 photometry based on observations acquired with TSU's T11 APT. These data were sufficient to investigate periodic signals that are a measurement of the stellar rotation period. Our analysis was able to disentangle the various aliases and isolate a rotation period of 89.3 ± 1.8 days. Our photometric precision and observing cadence are able to rule out transits of the two inner planets in the system, but the possibility of a transiting outer planet remains open.

Finally, our measured stellar parameters were used to derive the HZ boundaries of the system and investigate the location and dynamics of the planetary orbits with respect to the HZ. We find that, although the eccentric solution for planet c allows it to enter the optimistic HZ, the two inner planets are consistent with possible super-Venus planets (Kane et al. 2013, 2014). Long-term stability analysis shows that the system is stable in the current configuration, and that the eccentricity of the two inner planets frequently reduces to zero, at which times the orbit of planet c is entirely interior to the optimistic HZ. We thus conclude that the system is unlikely to host planets with surface liquid water.

G.W.H. acknowledges support from NASA, NSF, Tennessee State University, and the State of Tennessee through its Centers of Excellence program. T.S.B. acknowledges support from NASA grant 14-K2GO2_2-0075 and Louisiana State University. This work is based on observations obtained with the Georgia State University Center for High Angular Resolution Astronomy Array at Mount Wilson Observatory. The CHARA Array is supported by the National Science Foundation under Grant no. AST-1211929. Institutional support has been provided from the GSU College of Arts and Sciences and the GSU Office of the Vice President for Research and Economic Development. This research has made use of the Jean-Marie Mariotti Center `Aspro` service, available at www.jmmc.fr/aspro. This research has also made use of the following archives: the Exoplanet Orbit Database and the Exoplanet Data Explorer at exoplanets.org, the Habitable Zone Gallery at hzgallery.org, and the NASA Exoplanet Archive, which is operated by the California Institute of Technology, under contract with the National Aeronautics and Space Administration under the Exoplanet Exploration Program. The results reported herein benefited from collaborations and/or information exchange within NASA's Nexus for Exoplanet System Science (NExSS) research coordination network sponsored by NASA's Science Mission Directorate.

Software: `ASPRO` (http://www.jmmc.fr/aspro).

References

Anglada-Escudé, G., Amado, P. J., Barnes, J., et al. 2016, Natur, 536, 437
Astudillo-Defru, N., Bonfils, X., Delfosse, X., et al. 2016a, A&A, submitted
Astudillo-Defru, N., Delfosse, X., Bonfiles, X., et al. 2016b, A&A, in press (arXiv:1610.09007)
Avenhaus, H., Schmid, H. M., & Meyer, M. R. 2012, A&A, 548, A105
Bailey, J. I., III, White, R. J., Blake, C. H., et al. 2012, ApJ, 749, 16
Beichman, C. A., Neugebauer, G., Habing, H. J., & Clegg, P. E. 1988, Infrared Astronomical Satellite (IRAS) Catalogs and Atlases. Volume 1: Explanatory Supplement, NASA Ref. Publ. 1190, 1 (Washington, DC: NASA)
Bessel, M. S. 1990, A&A, 83, 357
Bohlin, R. C., Gordon, K. D., & Tremblay, P.-E. 2014, PASP, 126, 711
Boisse, I., Bonfils, X., & Santos, N. C. 2012, A&A, 545, A109
Boyajian, T., von Braun, K., Feiden, G. A., et al. 2015, MNRAS, 447, 846
Boyajian, T. S., von Braun, K., van Belle, G., et al. 2012, ApJ, 757, 112
Cantrell, J. R., Henry, T. J., & White, R. J. 2013, AJ, 146, 99
Chambers, J. E. 1999, MNRAS, 304, 793
Claret, A., & Bloemen, S. 2011, A&A, 529, A75
Corben, P. M., Carter, B. S., Banfield, R. M., & Harvey, G. M. 1972, MNSSA, 31, 7
Cousins, A. W. J. 1980a, SAAOC, 1, 166
Cousins, A. W. J. 1980b, SAAOC, 1, 234
Crossfield, I. J. M., Petigura, E., Schlieder, J. E., et al. 2015, ApJ, 804, 10
Cutri, R. M., Skrutskie, M. F., van Dyke, S., et al. 2003, yCat, 2246, 0
Davison, C. L., White, R. J., Henry, T. J., et al. 2015, AJ, 149, 106
Duncan, M. J., Levison, H. F., & Lee, M. H. 1998, AJ, 116, 2067
Eaton, J. A., Henry, G. W., & Fekel, F. C. 2003, in The Future of Small Telescopes in the New Millennium, Vol. II, ed. T. D. Oswalt (Dordrecht: Kluwer), 189
Gaidos, E., Mann, A. W., Kraus, A. L., & Ireland, M. 2016, MNRAS, 457, 2877
Gautier, T. N., III, Rieke, G. H., Stansberry, J., et al. 2007, ApJ, 667, 527
Hanbury Brown, R., Davis, J., Lake, R. J. W., & Thompson, R. J. 1974, MNRAS, 167, 475

Henden, A. A., Levine, S. E., Terrell, D., Smith, T. C., & Welch, D. 2012, JAVSO, 40, 430
Henry, G. W. 1999, PASP, 111, 845
Huber, D., Silva Aguirre, V., Matthews, J. M., et al. 2014, ApJS, 211, 2
Jenkins, J. S., Ramsey, L. W., Jones, H. R. A., et al. 2009, ApJ, 704, 975
Johnson, H. L. 1965, ApJ, 141, 170
Johnson, H. L., & Harris, D. L. 1954, ApJ, 120, 196
Kane, S. R., Barclay, T., & Gelino, D. M. 2013, ApJL, 770, L20
Kane, S. R., & Gelino, D. M. 2012, AsBio, 12, 940
Kane, S. R., Hill, M. L., Kasting, J. F., et al. 2016, ApJ, 830, 1
Kane, S. R., Kopparapu, R. K., & Domagal-Goldman, S. D. 2014, ApJL, 794, L5
Kasting, J. F., Kopparapu, R., Ramirez, R. M., & Harmen, C. E. 2014, PNAS, 111, 12641
Kasting, J. F., Whitmore, D. P., & Reynolds, R. T. 1993, Icar, 101, 108
Kilkenny, D., Koen, C., van Wyk, F., Marang, F., & Cooper, D. 2007, MNRAS, 380, 1261
Koen, C., Kilkenny, D., van Wyk, F., Cooper, D., & Marang, F. 2002, MNRAS, 334, 20
Koen, C., Kilkenny, D., van Wyk, F., & Marang, F. 2010, MNRAS, 403, 1949
Kopparapu, R. K., Ramirez, R., Kasting, J. F., et al. 2013, ApJ, 765, 131
Kopparapu, R. K., Ramirez, R., SchottelKotte, J., et al. 2014, ApJL, 787, L29
Laing, J. D. 1989, SAAOC, 13, 29
Léger, A., Defrère, D., Malbet, F., Labadie, L., & Absol, O. 2015, ApJ, 808, 194
Lindgren, S., Heiter, U., & Seifahrt, A. 2016, A&A, 586, A100
Mann, A. W., Feiden, G. A., Gaidos, E., Boyajian, T., & von Braun, K. 2015, ApJ, 804, 64
Mann, A. W., & von Braun, K. 2015, PASP, 127, 102
Mermilliod, J.-C. 1986, Catalogue of Eggen's UBV data
Mould, J. R., & Hyland, A. R. 1976, ApJ, 208, 399
Muirhead, P. S., Becker, J., Feiden, G. A., et al. 2014, ApJS, 213, 5
Muirhead, P. S., Hamren, K., Schlawin, E., et al. 2012, ApJL, 750, L37
Neves, V., Bonfils, X., Santos, N. C., et al. 2014, A&A, 568, A121
Newton, E. R., Irwin, J., Charbonneau, D., et al. 2016a, ApJ, 821, 93
Newton, E. R., Irwin, J., Charbonneau, D., Berta-Thompson, Z. K., & Dittmann, J. A. 2016b, ApJL, 821, L19
Niconov, V. B., Nekrasova, S. V., Polosuina, N. S., Rachkouvsky, N. D., & Chuvajev, W. K. 1957, IzKry, 17, 42
Önehag, A., Heiter, U., Gustafsson, B., et al. 2012, A&A, 542, A33
Paulson, D. B., Saar, S. H., Cochran, W. D., & Henry, G. W. 2004, AJ, 127, 1644
Queloz, D., Henry, G. W., Sivan, J. P., et al. 2001, A&A, 379, 279
Quintana, E. V., Barclay, T., Raymond, S. N., et al. 2014, Sci, 344, 277
Reid, N. 1982, MNRAS, 201, 51
Rojas-Ayala, B., Covey, K. R., Muirhead, P. S., & Lloyd, J. P. 2012, ApJ, 748, 93
Sturmann, J., ten Brummelaar, T. A., Ridgway, S. T., et al. 2003, Proc. SPIE, 4838, 1208
ten Brummelaar, T. A., McAlister, H. A., Ridgway, S. T., et al. 2005, ApJ, 628, 453
Turnbull, M. C. 2015, arXiv:1510.01731
van Leeuwen, F. 2007, A&A, 474, 653
Vanderburg, A., Plavchan, P., Johnson, J. A., et al. 2016, MNRAS, 459, 3565
Veeder, G. J. 1974, AJ, 79, 1056
von Braun, K., Boyajian, T. S., van Belle, G. T., et al. 2014, MNRAS, 438, 2413
Weis, E. W. 1984, ApJS, 55, 289
Weis, E. W. 1986, AJ, 91, 626
Weis, E. W. 1987, AJ, 93, 451
Weis, E. W. 1996, AJ, 112, 2300
Williams, D. M., & Pollard, D. 2002, IJAsB, 1, 61
Wright, D. J., Wittenmyer, R. A., Tinney, C. G., Bentley, J. S., & Zhao, J. 2016, ApJL, 817, L20